Correlation-based smoothing model for optical polishing

Yong Shu,[1] Dae Wook Kim,[2,*] Hubert M. Martin,[3] and James H. Burge[2,3]

[1]*College of Mechatronics and Automation, National University of Defense Technology, Changsha, Hunan 410073, China*

[2]*College of Optical Sciences, University of Arizona, Tucson, Arizona 85721, USA*

[3]*Steward Observatory, University of Arizona, Tucson, Arizona 85721, USA*

[*]*letter2dwk@hotmail.com*

Abstract: A generalized model is developed to quantitatively describe the smoothing effects from different polishing tools used for optical surfaces. The smoothing effect naturally corrects mid-to-high spatial frequency errors that have features small compared to the size of the polishing lap. The original parametric smoothing model provided a convenient way to compare smoothing efficiency of different polishing tools for the case of sinusoidal surface irregularity, providing the ratio of surface improvement via smoothing to the bulk material removal. A new correlation-based smoothing model expands the capability to quantify smoothing using general surface data with complex irregularity. For this case, we define smoothing as a band-limited correlated component of the change in the surface and original surface. Various concepts and methods, such as correlation screening, have been developed and verified to manipulate the data for the calculation of smoothing factor. Data from two actual polishing runs from the Giant Magellan Telescope off-axis segment and the Large Synoptic Survey Telescope monolithic primary-tertiary mirror were processed, and a quantitative evaluation for the smoothing efficiency of a large pitch lap and a conformal lap with polishing pads is provided.

OCIS codes: (220.0220) Optical design and fabrication; (220.4610) Optical fabrication; (220.5450) Polishing.

References and links

1. R. A. Jones, "Computer control for grinding and polishing," Photon. Spectra 34–39 (1963).
2. S. C. West, H. M. Martin, R. H. Nagel, R. S. Young, W. B. Davison, T. J. Trebisky, S. T. Derigne, and B. B. Hille, "Practical design and performance of the stressed-lap polishing tool," Appl. Opt. **33**(34), 8094–8100 (1994).
3. D. Golini, W. I. Kordonski, P. Dumas, and S. Hogan, "Magnetorheological finishing (MRF) in commercial precision optics manufacturing," Proc. SPIE **3782**, 80–91 (1999).
4. D. D. Walker, R. Freeman, R. Morton, G. McCavana, and A. Beaucamp, "Use of the 'Precessions'™ process for prepolishing and correcting 2D & 2(1/2)D form," Opt. Express **14**(24), 11787–11795 (2006).
5. D. W. Kim and J. H. Burge, "Rigid conformal polishing tool using non-linear visco-elastic effect," Opt. Express **18**(3), 2242–2257 (2010).
6. R. Angel, "Very large ground-based telescopes for optical and IR astronomy 4," Nature **295**(5851), 651–657 (1982).
7. R. Angel, "Future optical and infrared telescopes 3," Nature **409**(6818), 427–430 (2001).
8. H. M. Martin, R. G. Allen, J. H. Burge, D. W. Kim, J. S. Kingsley, K. Law, R. D. Lutz, P. A. Strittmatter, P. Su, M. T. Tuell, S. C. West, and P. Zhou, "Production of 8.4 m segments for the Giant Magellan Telescope," in Modern Technologies in Space-and-Ground-based Telescopes and Instrumentation II, Proc. SPIE **8450**, 84502D (2012).
9. J. H. Campbell, R. A. Hawley-Fedder, C. J. Stolz, J. A. Menapace, M. R. Borden, P. K. Whitman, J. Yu, M. Runkel, M. O. Riley, M. D. Feit, and R. P. Hackel, "NIF optical material and fabrication technologies: An overview," Proc. SPIE **5341**, 84–101 (2004).
10. D. W. Kim, W. H. Park, H. K. An, and J. H. Burge, "Parametric smoothing model for visco-elastic polishing tools," Opt. Express **18**(21), 22515–22526 (2010).

#193790 - $15.00 USD Received 15 Jul 2013; revised 5 Nov 2013; accepted 6 Nov 2013; published 14 Nov 2013

11. J. S. Taylor, G. E. Sommargren, D. W. Sweeney, and R. M. Hudyma, "The fabrication and Testing of Optics for EUV Projection Lithography," presented at the 23rd Annual International Symposium on Microlithography, Santa Clara, California, USA, 22–27 Feb. 1998.
12. D. W. Kim, S. W. Kim, and J. H. Burge, "Non-sequential optimization technique for a computer controlled optical surfacing process using multiple tool influence functions," Opt. Express **17**(24), 21850–21866 (2009).
13. N. J. Brown, P. C. Baker, and R. E. Parks, "The polishing-to-figuring transition in turned optics," SPIE's 25th Annual International Technical Symposium,(SPIE, 1982).
14. R. A. Jones, "Computer simulation of smoothing during computer-controlled optical polishing," Appl. Opt. **34**(7), 1162–1169 (1995).
15. P. K. Mehta and P. B. Reid, "A mathematical model for optical smoothing prediction of high-spatial frequency surface errors," in *Optomechanical Engineering and Vibration Control*, E. A. Derby, C. G. Gordon, D. Vukobratovich, P. R. Yoder Jr., and C. H. Zweben, eds., Proc. SPIE **3786**, 447 (1999).
16. M. T. Tuell, J. H. Burge, and B. Anderson, "Aspheric optics: smoothing the ripples with semiflexible tools," Opt. Eng. **41**(7), 1473–1474 (2002).
17. D. W. Kim, H. M. Martin, and J. H. Burge, "Control of Mid-spatial-frequency Errors for Large Steep Aspheric Surfaces," in Optical Fabrication and Testing (OF&T) Technical Digest (Optical Society of America, Washington, DC), OM4D.1 (2012).
18. P. Su, R. E. Parks, L. Wang, R. P. Angel, and J. H. Burge, "Software configurable optical test system: a computerized reverse Hartmann test," Appl. Opt. **49**(23), 4404–4412 (2010).

1. Introduction

Various Computer Controlled Optical Surfacing (CCOS) processes have been developed for different applications since the 1960s [1–5]. Many advanced precision optics, such as large aspheric mirrors for next generation telescopes [6–8] and super smooth optics for high power laser systems [3, 9], have been manufactured to superior optical quality based on the deterministic material removal of the CCOS processes.

One key component of CCOS is the Tool Influence Function (TIF), which is the spatial distribution of material removal under a polishing tool. Most CCOS processes distribute and accumulate their TIFs over the optic to achieve a desired removal, which is often the error map of an optical surface. Thus, a stable and deterministic TIF is critical for a successful CCOS process.

Smoothing during optical polishing is one of the most critical and important topics in the optical fabrication field today [10]. As modern CCOS processes target a structure function or Power Spectral Density (PSD) specification of the optics, which is directly related to the final system performance such as sharpness of the point spread function, control of mid- to high-spatial-frequency surface error becomes a critical issue [9, 11] and the deterministic control of these error components often determines the overall convergence of CCOS processes.

The TIF is strongly related to polishing parameters such as pressure distribution under the tool, rigidity of the tool, polishing interface material, and tool motion. Maintaining an intimate contact between the tool and workpiece is very important to achieving a deterministic TIF [5].

Some rigidity in a tool is also desired to get smoothing effects. For instance, an infinitely rigid tool does not conform to the small scale surface irregularities, and it only sits on the high peaks as depicted in Fig. 1 (left). As the tool moves on the surface it wears down the peaks, and the surface is smoothed out as shown in Fig. 1 (right).

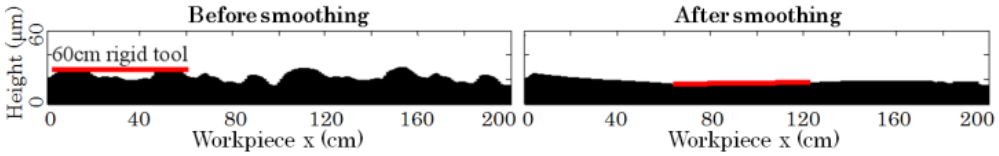

Fig. 1. Smoothing simulation for a 60cm infinitely rigid tool [10].

There are two main approaches to control small scale errors. The first approach is direct figuring utilizing very small tools [12] with control of dwell time (or pressure or stroke speed)

#193790 - $15.00 USD Received 15 Jul 2013; revised 5 Nov 2013; accepted 6 Nov 2013; published 14 Nov 2013

as a function of position. This method is very effective since it removes materials mainly where the surface error is high, but it requires an accurate target error map and accurate tool positioning to avoid tool marks on the optics. The second approach used the natural smoothing effect of a polishing tool that is larger than the features. As it automatically removes mid- to high-spatial-frequency errors, smoothing is an attractive solution to produce a high quality smooth optic. However, the smoothing effect is not easy to predict and evaluate quantitatively, as required to achieve a deterministic process for rapid convergence.

A smoothing model for an elastic backed lapping belt was introduced by Brown and Parks in 1981 [13]. Jones analyzed the smoothing effect of a pitch tool later [14], and the bridging model was applied to study the smoothing effect of a flexible polishing tool by Mehta and Reid [15]. Tuell further improved the bridging model via a Fourier decomposition approach in 2002 [16]. Based on measured experimental data under controlled conditions, Kim *et al*. developed a parametric smoothing model to quantify the smoothing efficiency of various polishing processes [10]. This step was useful because it allowed an apples-to-apples quantitative comparison of different processes, but it was limited to the special case of sinusoidal ripples in the surface.

We now present a generalized parametric smoothing model that overcomes these limitations. For the first time, the newly developed correlation-based smoothing model allows us not only to evaluate, but also to predict the smoothing effects during actual CCOS processing of real surfaces that have random topology. Such a parametric model is necessary to simplify the data processing and provide a quantitative assessment of the surface improvement from natural smoothing. This information is used to optimize the fabrication process to balance surface quality and fabrication time.

This paper presents background, introduces a methodology for processing data, and demonstrates performance of this method. A brief review of the original parametric smoothing model is given in Section 2. The new correlation-based model is introduced in Section 3, and some actual data from CCOS runs are presented and analyzed in Section 4.

2. Background knowledge

2.1 Parametric smoothing model

The parametric model to describe smoothing effects for sinusoidal surface errors was introduced in 2010 [10]. This model for sinusoidal ripples defines a smoothing factor *SF* to describe the smoothing efficiency, which was defined as $\Delta\varepsilon/\Delta z$, where $\Delta\varepsilon$ is the difference between Peak-to-Valley (PV) values of the sinusoidal ripples before and after the smoothing run, and Δz is the nominal removal depth as depicted in Fig. 2. (Note: Ideally, smaller Δz for each evaluation step works better as it produces more accurate instantaneous smoothing factor at the initial surface error ε_{ini} (*i.e.* PV of $Profile_{initial}$). Using too large Δz will underestimate the smoothing factor.)

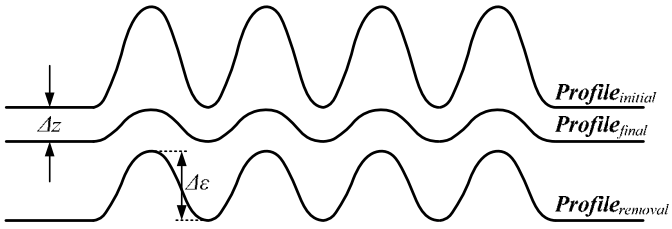

Fig. 2. The sinusoidal ripple profiles: initial, final and removal (*i.e.* initial – final).

The smoothing factor depends on the initial surface error ε_{ini} and that dependence can be parameterized as

#193790 - $15.00 USD Received 15 Jul 2013; revised 5 Nov 2013; accepted 6 Nov 2013; published 14 Nov 2013

$$SF = k \cdot (\varepsilon_{ini} - \varepsilon_0) \quad (1)$$

where k is the sensitivity to initial error and ε_0 is the minimum error for which smoothing can happen [17].

Using the parametric smoothing model in Eq. (1), a polishing tool's smoothing capability was shown to have linear dependence on ε_{ini}. The two parameters k and ε_0 can be determined by performing a few sets of experimental smoothing runs. This parametric model to evaluate and compare various tools' smoothing characteristics was successfully verified with experimental data [10].

2.2 Stressed lap and Rigid Conformal lap

The stressed lap and Rigid Conformal (RC) lap are the tools that have been employed for various large optics CCOS projects at the University of Arizona as shown in Fig. 3.

Fig. 3. Computer controlled polishing machines equipped with the 0.8m (contact area diameter) stressed lap on the 8.4m diameter Large Synoptic Survey Telescope monolithic primary-tertiary workpiece (left) and the 0.25m diameter RC lap on the 8.4m diameter Giant Magellan Telescope off-axis segment (right) at the Steward Observatory Mirror Lab, University of Arizona [8].

The stressed lap [2] consists of a stiff aluminum plate that is bent actively by actuators mounted at its edge. The polishing interface may be pitch or polyurethane pads. The bending actuators control the shape of the polishing surface to match the local surface of the aspheric mirror.

The RC lap is constructed with solid back plate, non-Newtonian fluid and polishing interface material (*e.g.* polyurethane pad). The tool automatically conforms to a free-form surface, but is stiff on short time scales, due to its unique visco-elastic behavior [5, 8].

3. Correlation-based smoothing model

The correlation-based smoothing model was developed to analyze smoothing effects for irregular (*e.g.* non-sinusoidal) surface errors of actual CCOS runs. The original model in Section 2.1 works well for the well-defined sinusoidal ripple cases with relatively large ripple amplitude compared to the measurement noise. However, for actual CCOS data, the measured surface map contains errors over a wide range of spatial frequencies and the amplitude of the data where smoothing happens may be comparable to the measurement noise or uncertainty.

The data processing flow of the correlation-based smoothing model is shown in Fig. 4. To separate the low- and high-spatial-frequency components from the measured initial and final surface map spatial-frequency filtering is applied with a cut-off spatial frequency f_{cutoff} . The difference map between the high-pass filtered maps contains the smoothing information. The difference between the low-pass filtered maps represents the nominal removal map, which is a 2-dimensional version of Δz in Section 2.1. The maps are divided into N common circular sub-regions, which are $2/f_{cutoff}$ in diameter, to evaluate local smoothing effects. The number of sub-regions N is chosen to cover the whole map without missing areas or to cover some interesting local sections (e.g. mirror edges) in the map. All N sub-region pairs in the high-pass filtered initial and difference map are scanned, and the correlation coefficient ρ for each pair (initial and difference map) is calculated. If the coefficient exceeds a threshold $\rho_{threshold}$, the

#193790 - $15.00 USD Received 15 Jul 2013; revised 5 Nov 2013; accepted 6 Nov 2013; published 14 Nov 2013

sub-regional smoothing factor *SF* is calculated. Once the scanning is completed all *SF* values are plotted together, and the linear smoothing rate can be evaluated. Details of each step are given in Section 3.1-3.3.

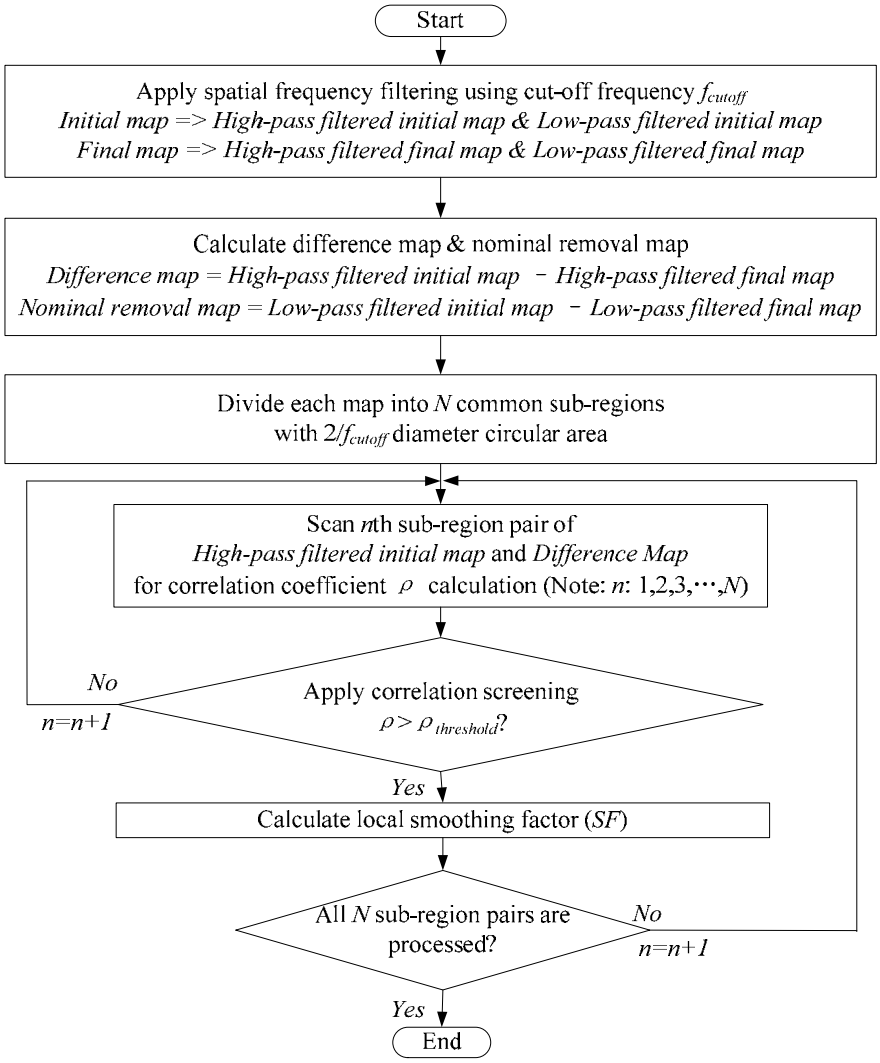

Fig. 4. Data processing flow of the correlation-based smoothing model.

3.1 Spatial frequency filtering

Figuring (removing errors using deterministic means such as dwell time control) and smoothing often occur simultaneously all over the workpiece during a CCOS run. Figuring happens on low-spatial-frequency errors (*i.e.* features larger than the tool size) while smoothing takes place on mid- to high-spatial-frequency errors. In order to evaluate the smoothing effects separated from the figuring, a high-pass spatial filtering is applied to the raw surface map data. The filtered maps include the information about smoothing. The cut-off spatial frequency f_{cutoff} depends on the frequency range of interest for the smoothing evaluation, and is typically around 1 / half the tool size.

It is important to note that smoothing is generally a function of spatial frequency. The smoothing factors presented in this study, which uses high-pass filtering, result from a

#193790 - $15.00 USD Received 15 Jul 2013; revised 5 Nov 2013; accepted 6 Nov 2013; published 14 Nov 2013

superposition of individual smoothing effects entangled with various spatial frequency errors. For some applications, it may be useful to apply different band-pass spatial filters (*e.g.* f_{min}-f_{max}) to evaluate smoothing effects over certain ranges of spatial frequency.

3.2 Correlation screening

As different degrees of smoothing happen at various locations on a workpiece, all sub-regions used to evaluate the local smoothing factor must be at places where actual smoothing occurred. The difference map (high-pass filtered initial map – high-pass filtered final map) should look similar to the high-pass filtered initial map. In other words, more removal should happen at the high locations in the initial surface.

Two example cases showing well and badly correlated profiles are shown in Fig. 5. The initial and difference profiles are similar with a scale factor for the well correlated case, which indicates efficient smoothing. For the badly correlated case, the two profiles do not match.

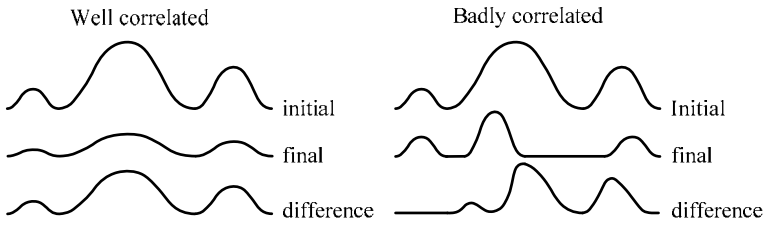

Fig. 5. Comparison between well correalated profiles (left) and badly correlated profiles (right).

A correlation screening is introduced for the smoothing-or-not test. The correlation coefficient ρ between the high-pass filtered initial map $M_{ini}(x,y)$ and the difference map $M_{diff}(x,y)$ in a sub-region pair is defined as:

$$\rho_{M_{ini},M_{diff}} = \frac{\iint_{sub-region}(M_{ini}(x,y)-\overline{M_{ini}})(M_{diff}(x,y)-\overline{M_{diff}})dxdy}{\sqrt{\iint_{sub-region}(M_{ini}(x,y)-\overline{M_{ini}})^2 dxdy \iint_{sub-region}(M_{diff}(x,y)-\overline{M_{diff}})^2 dxdy}}$$
$$= \frac{\iint_{sub-region}(M_{ini}(x,y)-\frac{\iint_{sub-region}M_{ini}(x,y)dxdy}{\iint_{sub-region}dxdy})(M_{diff}(x,y)-\frac{\iint_{sub-region}M_{diff}(x,y)dxdy}{\iint_{sub-region}dxdy})dxdy}{\sqrt{\iint_{sub-region}(M_{ini}(x,y)-\frac{\iint_{sub-region}M_{ini}(x,y)dxdy}{\iint_{sub-region}dxdy})^2 dxdy \iint_{sub-region}(M_{diff}(x,y)-\frac{\iint_{sub-region}M_{diff}(x,y)dxdy}{\iint_{sub-region}dxdy})^2 dxdy}}. \quad (2)$$

A correlation coefficient of 1 means the two maps are the same with a scale factor. We reduce the influence of measurement noise and other polishing effects by evaluating regions with correlation coefficient above some threshold value. The choice of this threshold depends primarily on the quality of the data.

The correlation coefficient needs to be higher than a pre-set threshold $\rho_{threshold}$ (*e.g.* 0.5), which may depend on various factors such as measurement noise, in order to pass the screening. Only the qualified sub-regions are employed for the local *SF* calculation. This is a critical step to distinguish smoothing from the other effects such as measurement uncertainty and tool misfit, which may also affect the measured surface data. We acknowledge that the definition of smoothing in this study is limited to the case described in Section 2.1 and 3.2. Smoothing due to a different mechanism (e.g. badly correlated initial and difference map, but smoother final map) could still be analyzed by applying smaller (i.e. less rigorous) $\rho_{threshold}$ values, but with compromised reliability of the model.

#193790 - $15.00 USD Received 15 Jul 2013; revised 5 Nov 2013; accepted 6 Nov 2013; published 14 Nov 2013

3.3 General smoothing factor

The original definition of smoothing factor [10] was based on PV values of the initial and final profiles. A sinusoidal surface error, which is ideal to evaluate the smoothing effect in an experimental set-up, was well represented by the PV. However, an irregular surface error map is a superposition of various frequencies and amplitudes.

As Root-Mean-Square (RMS) is a statistical measure of data over a certain area, the general smoothing model utilizes RMS values to represent the surface error ε in Eq. (1). In other words, the sub-regional RMS values of the high-pass filtered initial and final map are used in the general *SF* equation. Also, the nominal removal depth Δz often cannot be measured, so it is replaced with the average value of the nominal (or predicted) removal in the sub-region. The original *SF* equation [10] is now rewritten as a general *SF* equation

$$SF = \frac{RMS_{high-pass\_filtered\_initial\_map} - RMS_{high-pass\_filtered\_final\_map}}{Average_{nominal\_removal\_map}} = \frac{\sqrt{\iint_{sub-region} M_{ini}^{2}(x,y)dxdy \Big/ \iint_{sub-region} dxdy} - \sqrt{\iint_{sub-region} M_{fin}^{2}(x,y)dxdy \Big/ \iint_{sub-region} dxdy}}{\iint_{sub-region} M_{nominal}(x,y)dxdy \Big/ \iint_{sub-region} dxdy}, \quad (3)$$

where M_{ini} and M_{fin} are the high-pass filtered initial and final maps, $M_{nominal}$ is the nominal (or predicted) removal map, and *sub-region* is the local area under evaluation. The local *SF* values at various sub-regions on a workpiece are calculated using Eq. (3) and plotted to evaluate the smoothing efficiency of an actual CCOS process.

4. Smoothing evaluation using the correlation-based smoothing model

4.1 Local smoothing study via correlation screening

The local smoothing for CCOS polishing was studied using the correlation screening. The 8.4m Giant Magellan Telescope (GMT) off-axis segment was manufactured and completed by polishing with a stressed lap and RC laps, primarily a 0.8m stressed lap and a 0.25m RC lap [8]. The stressed lap was mainly used to correct low-spatial-frequency errors, while RC lap was used to directly figure the mid-spatial-frequency errors via dwell time control. Besides the figuring, features smaller than the RC lap were expected to be smoothed out during both stressed lap and RC lap runs.

Two GMT surface measurement data sets for each tool were analyzed to study the local smoothing effects. As described in Section 3.2, the correlation coefficient ρ between the high-pass filtered initial map and difference map represents the likelihood of smoothing events. Three exemplary sub-region pairs of the high-pass filtered (f_{cutoff} = 1/150mm) initial map and difference map with different correlations are presented in Fig. 6. The size of sub-regions is 0.3m in diameter (*i.e.* 2/ f_{cutoff}), and the irregular removal shapes in difference maps cannot be from the direct figuring (using >0.25m diameter tools). The similarity between the high-pass filtered initial map and difference map clearly increases as the correlation coefficient increases, showing that smoothing happens locally where the correlation coefficients are high.

#193790 - $15.00 USD Received 15 Jul 2013; revised 5 Nov 2013; accepted 6 Nov 2013; published 14 Nov 2013

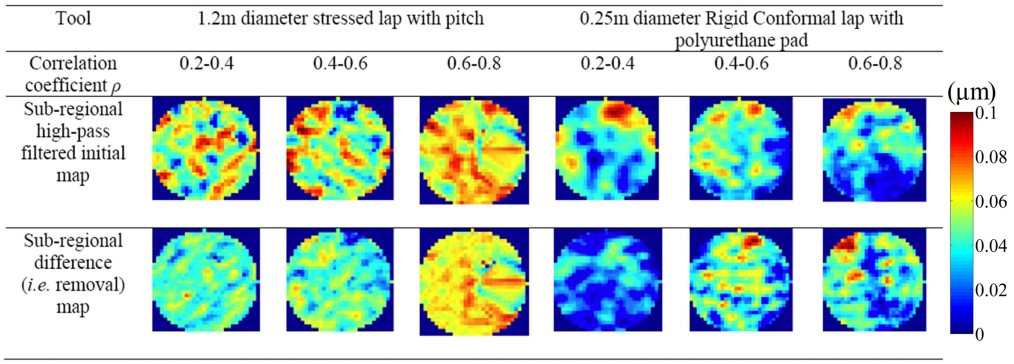

Fig. 6. Six exemplary sub-region surface maps showing the local smoothing event for different correlation coefficients. The sub-regions are 0.3m in diameter on the 8.4m GMT segement. *(Note: Red means high in the high-pass filtered initial map and more removal in the difference map.)*

4.2 Linear smoothing effect for sinusoidal error case

The linearity of smoothing effects on a well-defined sinusoidal error was verified with the original smoothing model [10] and re-confirmed using the new correlation-based smoothing model. An ideal smoothing experiment using a 100mm diameter RC lap (with LP-66 polyurethane pads) on a 200mm Pyrex substrate with sinusoidal surface error ripples was conducted by following the procedures for the original model [10]. The correlation-based model was applied to analyze the data, and the calculated *SF* values are plotted in Fig. 7.

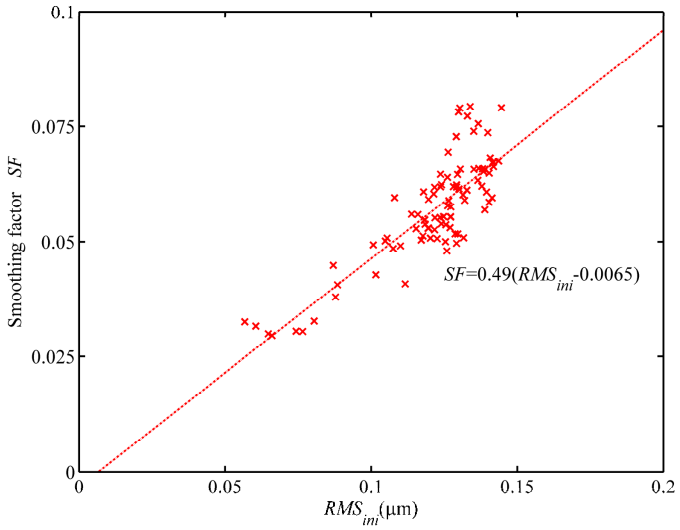

Fig. 7. Smoothing factor *SF vs.* initial sinusoidal error RMS_{ini} for a RC lap with LP-66 polyurethane pad on a Pyrex workpiece.

The data points show the expected linear trend between RMS_{ini} and *SF*. For this particular sinusoidal smoothing run using the RC lap with LP-66, the slope of the *SF* graph is 0.49 μm^{-1} and the limiting amplitude for any smoothing occur is about 5-10nm rms. This case study shows that the newly introduced general model, as expected, still works for the specific sinusoidal error cases.

#193790 - $15.00 USD Received 15 Jul 2013; revised 5 Nov 2013; accepted 6 Nov 2013; published 14 Nov 2013

4.3 Smoothing evaluation for actual CCOS runs

Four sets of measured surface data for two actual CCOS projects, mirrors for the GMT and the Large Synoptic Survey Telescope (LSST), were processed using the correlation-based smoothing model. Detailed CCOS parameters are presented in Table 1.

Table 1. CCOS parameters for the GMT and LSST runs

	Case 1		Case 2	
Project	GMT off-axis primary segment		LSST monolithic primary-tertiary mirror	
Polishing compound	Rhodite 906		Rhodite 906	
Workpiece diameter	8.4m		5.066m (for tertiary)	
Metrology	Interferometer using Computer Generated Hologram [8]		Software Configurable Optical Test System [18]	
Polishing tool type	250mm dia. RC lap	1200mm dia. Stressed lap	350mm dia. RC lap	800mm dia. Stressed lap
Tool interface with workpiece	LP-66 polyurethane pad	Pitch	LP-66 polyurethane pad	LP-66 polyurethane pad on pitch

For the four data sets, all the sub-regions were scanned and checked with the correlation coefficient screening, and the local smoothing factors were calculated. Common data processing parameter values including f_{cutoff} = 1/150mm were used during the calculation for a fair comparison. Instead of applying a fixed $\rho_{threshold}$ value, the correlation coefficient ρ distribution has been studied, and the mean ρ_{mean} and standard deviation $\rho_{standard\_deviation}$ of the histogram were calculated. By setting $\rho_{threshold} = \rho_{mean} - \rho_{standard\_deviation}$, most of the local areas (*e.g.* >~85% for normal distribution) were involved in the SF evaluation process. Also, ρ_{mean} provides additional information indicating the degree of ideal smoothing during the CCOS runs. For instance, as an extreme case, ρ_{mean} would be 1 if all the local smoothing actions were ideal cases. As described earlier, these parameter values may vary depending on the spatial frequency range of interest or limitations such as measurement noise level. The processed *SF* values with histograms showing ρ distribution are plotted in Figs. 8 and 9.

For the GMT polishing run data set (Case 1, Fig. 8), the 1.2m stressed lap with pitch showed ~10 times steeper *SF* slope than the 0.25m RC lap. Although there may be some other factors (*e.g.* lap misfit) affecting the smoothing efficiency, these data agree with the results of controlled experiments with sinusoidal surface errors, which showed a much steeper SF slope for a conventional pitch lap compared to the RC lap with polyurethane pad [10]. The correlation coefficient histograms in Fig. 8 (right) show the distribution of calculated ρ values in all the sub-region pairs. Both the stressed lap and the RC lap case are highly biased toward positive correlation coefficients. This non-symmetric distribution provides a good confirmation that the evaluated smoothing cases are not governed by random or uncorrelated errors in the measurements. For instance, if the difference between initial and final map was mainly caused by random noise, the distribution must be centered around ρ = 0. The mean ρ value with standard deviation was 0.381 ± 0.135 for the stressed lap and 0.433 ± 0.107 for the RC lap.

#193790 - $15.00 USD Received 15 Jul 2013; revised 5 Nov 2013; accepted 6 Nov 2013; published 14 Nov 2013

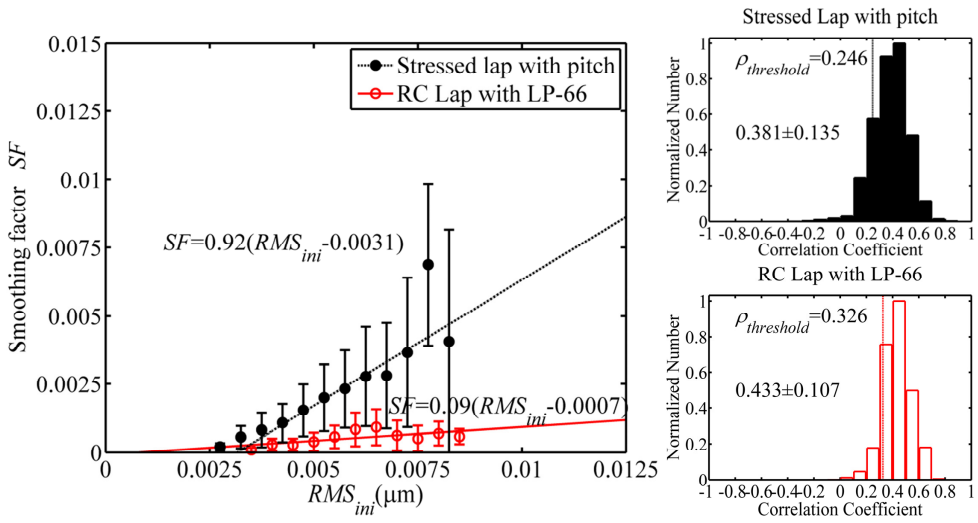

Fig. 8. Smoothing factor (left) and correlation coefficient ρ histogram (right) for Case 1: 8.4m GMT off-axis primary workpiece, *SF vs.* RMS_{ini} for 1.2m stressed lap with pitch (black solid circle) and 0.25m RC lap with polyurethane pad (red open circle). (The bar represents the spread (+/– standard deviation) of the local *SF* values. The values in the histogram are the mean+/–standard deviation of the distribution. The $\rho_{threshold}$ value is indicated as a vertical thin line in the histogram.)

The processed LSST surface data (Case 2, Fig. 9) showed that the 0.8m stressed lap with polyurethane pad on pitch gives ~1.2 times steeper *SF* slope than the 0.35m RC lap with the same polyurethane pad.

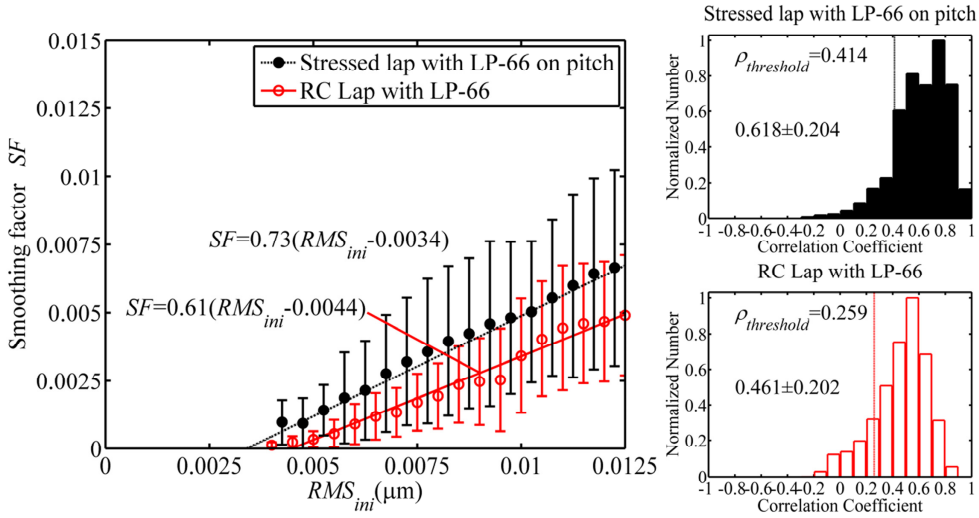

Fig. 9. Smoothing factor (left) and correlation coefficient ρ histogram (right) for Case 2: 5.066m LSST tertiary mirror, *SF vs.* RMS_{ini} for 0.8m stressed lap with pitch and LP-66 polyurethane pad (black solid circle) and 0.35m RC lap with polyurethane pad (red open circle). (The bar represents the spread (+/– standard deviation) of the local *SF* values. The values in the histogram are the mean+/–standard deviation of the distribution. The $\rho_{threshold}$ value is indicated as a vertical thin line in the histogram.)

Similar to Case 1, the ρ histogram showed well biased correlation coefficient distributions, $\rho = 0.618 \pm 0.204$ for the stressed lap and $\rho = 0.461 \pm 0.202$ for the RC lap. (In practice, this histogram may provide a guideline to set a $\rho_{threshold}$ value.) An absolute comparison between

#193790 - $15.00 USD Received 15 Jul 2013; revised 5 Nov 2013; accepted 6 Nov 2013; published 14 Nov 2013

Cases 1 and 2 is not valid, as many other factors like tool size and method of measurement were not the same. However, the relative difference of *SF* slope between the RC lap and the stressed lap was significantly smaller than for Case 1 where the stressed lap was faced with pitch. This result reveals the negative effect of placing the polyurethane pad on pitch in terms of smoothing efficiency.

The linearity of the *SF* graphs and the validity of the new smoothing model as an objective method to evaluate and compare different CCOS processes were well confirmed and demonstrated for these two cases studied.

5. Conclusion

A generalized smoothing model eliminating some limitations of the previous parametric smoothing model was developed to describe and understand realistic smoothing effects for various CCOS processes. Some previous models provide an excellent insight to select optimal smoothing tool design parameters using an iterative simulation approach [14] and a very convenient way to assess a specific tool's smoothing capacity from an experimental set-up with sinusoidal ripples [10]. However, they couldn't be applied to actual polishing cases with arbitrary initial and final error shapes, which must be analyzed and evaluated based on the measured data for the optimization and improvement of actual CCOS processes.

Newly developed methods of processing data for the *SF* calculation, such as correlation screening, have been demonstrated. Except for Eq. (3) in Section 3.3, modified from the previous parametric model [10], all other parts of the present model—including the spatial filtering process to distinguish smoothing from figuring removal, the correlation-based threshold to judge the likelihood of smoothing, and the final data analysis utilizing the correlation coefficient statistics—has been developed and presented for the first time.

The presented model was carefully verified using real polishing data at various levels throughout Section 4.1-4.3 in series. Measured surface maps of the 8.4m GMT off-axis segment and the 5.066m LSST tertiary mirror were processed, and the quantitative smoothing evaluation for two different types of tools has been successfully performed. The actual polishing parameters are all provided with sufficient details for the reproduction of the results and its general use by others in the field.

From the result we can conclude that: i) the correlation-based smoothing model can analyze and quantitatively describe the smoothing effect for actual CCOS data, ii) the stressed lap with pitch smooths faster than the RC lap with polyurethane pad, and iii) the polyurethane pad on pitch degrades the smoothing capability of the bare pitch tool. This general model, which breaks the boundary of the original model's application limited to the experimental cases and unlocks the new access to real optics fabrication for the first time, provides a systematic way to evaluate or develop CCOS processes to achieve higher convergence rates and superior surface error control in the mid- to high-spatial-frequency range.

The correlation-based smoothing model can serve as a unique and powerful smoothing data processing method in the field. This model allows quantitative evaluation and comparison between different polishing processes and tools. Previous assessments of the effectiveness were made using limited test cases, or they were made based on subjective observations. As this model allows analyzing any general CCOS data, this model will add a great value to the precision optical fabrication community who wants to develop and test various smoothing approaches and to report their technical advances using a quantitative model. Also, the application of the method developed here is expected to allow optical fabricators to optimize their tools and processes.

Acknowledgments

This study was funded by the Chinese Scholarship Council (CSC). The first author conducted this research at the Large Optics Fabrication and Testing group, College of Optical Sciences, as a visiting scholar at the University of Arizona. Also, this material is based in part upon work

supported by the Association of Universities for Research in Astronomy (AURA) through the National Science Foundation under Scientific Program Order No. 10 as issued for support of the Giant Segmented Mirror Telescope for the United States Astronomical Community, in accordance with Proposal No. AST-0443999 submitted by AURA. In addition, LSST project activities are supported in part by the National Science Foundation through Governing Cooperative Agreement 0809409 managed by AURA, and the Department of Energy under contract DE-AC02-76-SFO0515 with the SLAC National Accelerator Laboratory. Additional LSST funding comes from private donations, grants to universities, and in-kind support from LSSTC Institutional Members. The authors would also like to thank Francois Piche at QED for the valuable input.

#193790 - $15.00 USD Received 15 Jul 2013; revised 5 Nov 2013; accepted 6 Nov 2013; published 14 Nov 2013